# Phenomenological Lagrangian approach to two kaon photoproduction and pentaquark searches

W. Roberts

*Department of Physics, Old Dominion University, Norfolk, Virginia 23529, USA*
*and Thomas Jefferson National Accelerator Facility, 12000 Jefferson Avenue, Newport News, Virginia 23606, USA*
(Received 16 August 2004; published 10 December 2004)

We examine cross sections for the processes $\gamma N \rightarrow N K \bar{K}$ in the framework of a phenomenological Lagrangian. We include contributions from $\Lambda$ and $\Sigma$ resonances up to spin $3/2$, as well as those from an exotic $\Theta^+$. We allow the $\Theta^+$ to have spin $1/2$ or $3/2$, with either positive or negative parity in each case. We also allow the state to be either isovector or isoscalar. We find that the scenario that most closely matches observations at Jefferson Laboratory requires a moderately large coupling of the $\Theta^+$ to $NK^*$.

## I. INTRODUCTION

### A. Experimental indications

In the past several months, a number of experimental groups have reported signals for a pentaquark state called the $\Theta^+$ [1–9]. The first evidence for such a state was reported by the Spring-8 Collaboration [1]. The search by Spring-8 was motivated by predictions, made within the framework of the chiral soliton model, by Diakonov *et al.* [10]. Most searches that have reported evidence for the state put its mass around 1540 MeV. However, in all cases, the experimental resolution has been such that only upper limits for the width of the state could be given. Evidence for other pentaquarks predicted as partners to the $\Theta^+$, particularly the $\Xi^{--}$, has also been reported by the NA49 Collaboration [11]. Using the time-delay technique, Kelkar *et al.* have found evidence of not only the $\Theta^+$ in $K^+N$ scattering data, but also a possible spin-orbit partner [12] along with a third possible state.

Despite the number of pentaquark sightings, the situation is far from clear. Two members of the NA49 Collaboration produced a minority report pointing out that there was no strong evidence for the existence of the $\Xi^{--}$ in older, higher-precision data [13]. The HERA-B Collaboration sees no evidence for the $\Theta^+$ [14], and the BES Collaboration also report no evidence in their searches [15]. Searches at RHIC have also yielded no evidence so far [16]. Because some experiments have reported signals for the pentaquarks, while others have seen no sign of them, Karliner and Lipkin [17] have postulated the existence of a "crypoexotic" $N^*$ that plays a significant role in production of the $\Theta^+$. In addition, none of the experiments that report a signal for any of the pentaquarks can say anything about their spin or parity.

Quite apart from the question of the existence of the $\Theta^+$, the question of its width is also very interesting. Nussinov [18] has examined the implication of such a state for existing $K^+d$ data, and has concluded that the width of the state had to be less than 6 MeV. Arndt and collaborators [19] have performed a similar analysis on $K^+N$ scattering data, and have concluded that the width has to be less than 1 MeV, while Haidenbauer and Krein [20] conclude that the width of the state must be less than 5 MeV, or that its mass must be much lower than reported. Cahn and Trilling [21] have suggested that the width is $0.9 \pm 0.3$ MeV, based on their analysis of

data from $K^+$ collisions on xenon. Gibbs [22] has also examined $K^+d$ data and has extracted a width of $0.9 \pm 0.2$ MeV. Sibirtsev *et al.* [23] have come to similar conclusions.

### B. Theoretical implications

The existence of a pentaquark state would not be too jarring for most QCD practitioners, as multiquark states have been anticipated for decades. However, its light mass and apparently narrow width are difficult to explain in a "conventional" scenario, and have stimulated much discussion and many postulates. Dzierba *et al.* have raised the possibility that the "signal" is really a kinematic reflection [24]. Jaffe and Wilczek [25] have constructed a diquark scenario for the $\Theta^+$. One consequence of their scenario is that the state should have a spin-orbit partner, for which there is little or no evidence to date. Capstick and collaborators [26] have suggested that the state is as narrow as it is because it has isospin 2. This means that there should be isospin partners, none of which have been seen.

Jennings and Maltman [27] have examined pentaquark phenomenology in a number of scenarios, and conclude that such a state fits into the quark model picture if its parity is positive, but this implies the existence of spin-orbit partners. Karliner and Lipkin [28] invoke the mixing of two nearly degenerate $KN$ resonances to explain the narrow width of the $\Theta^+$. They have also speculated on the phenomenology of pentaquark states containing a charm quark [29]. In addition, there are many papers that examine the phenomenology of pentaquarks using QCD sum rules [30], various quark models [31], and string theory [32]. A number of unique scenarios have also been proposed [33]. There have even been suggestions that the states seen are in fact heptaquarks [34], or $NK\pi$ bound states [35]. Some lattice simulations suggest that the parity of the state is negative [36,37], while the work of Chiu and Hsieh suggests that it is positive [38]. More recent lattice work reports no signal for the pentaquark state [39].

### C. Cross-section ramifications

Among the many unanswered questions regarding the $\Theta^+$ (and other pentaquark candidates) is that of the cross section

for its production in a particular reaction. To address this, a number of authors have examined cross sections for producing them in a number of reactions [40–49]. Most of these have been aimed at determining the spin and parity of the state, but they have all provided estimates for the production cross section. Various photoproduction mechanisms and observables are examined in Refs. [40–49], while the authors of Ref. [42] treat the reaction $K^+ p \rightarrow \pi^+ K^+ n$ with kinematics suited to production of the $\Theta^+$. The authors of Ref. [45] also examine production of the $\Theta^+$ using a pion as the incident particle.

The calculation of Ref. [49] is closest in spirit to the work that we present here. Those authors use a phenomenological Lagrangian to describe the reaction $\gamma n \rightarrow n K^+ K^-$. In addition to the contribution of the $\Theta^+$, they also included two $\Sigma^-$ hyperons: the $\Sigma^-(1197)$ and the $\Sigma^-(1660)$. These hyperons provided the background contribution in their calculation. Close and Zhao [41] have emphasized the importance of comparing the cross section for producing the pentaquark states with those for producing nonexotic hyperons.

In this paper, we examine the cross section for the process $\gamma N \rightarrow N K \bar{K}$. We include many contributions, and examine all of the channels that are allowed. By including a number of contributions, we are able to understand the roles played by nonexotic hyperons, and by the $\phi(1020)$. More specifically, since some of the properties of the nonexotic hyperons are known, these can be used to get a handle on how big are the cross sections for their production, and for the production of the $\Theta^+$.

The results of this calculation are relevant to past, presnt, and future searches using photon beams. For the published results so far, this means the searches at JLab [3,5], the search by the Saphir Collaboration [4], and, of course, the search by the Spring-8 Collaboration [1]. We note, however, that in Ref. [5], the process studied is $\gamma p \rightarrow n \pi^+ K^+ K^-$, not any of the ones discused in this paper. While the main focus of our discussion will be the JLab searches, we will also comment on the other two searches where appropriate.

The rest of this paper is organized as follows. The next two sections focus on establishing the framework for the calculation: the general amplitude, kinematics, and cross section are discussed in the next section, and the phenomenological Lagrangian terms and most of the coupling constants needed for building the model are presented in Sec. III. The diagrams representing the contributions that are included in this calculation are also shown in that section. We present our results in Sec. IV, and a summary and outlook in Sec. V.

## II. GENERAL AMPLITUDE, KINEMATICS, AND CROSS SECTION

### A. Kinematics and cross section

We begin by describing the kinematics of the process. $k$ is the momentum of the photon, $p_1$ is that of the target nucleon, $p_2$ is that of the scattered nucleon, and $q_1$ and $q_2$ are the kaon momenta. Momentum conservation gives

$$k + p_1 = p_2 + q_1 + q_2. \quad (1)$$

This means that when we construct the amplitude for the process using all the four-vectors at our disposal, we can eliminate one of these from consideration.

The total center-of-mass energy of the process is $\sqrt{s}$, where $s = (k + p_1)^2$. We may define a variable $t$ as the square of the momentum transfered to the nucleon, namely $t = (p_2 - p_1)^2$, and this is related to the scattering angle of the nucleon in the center-of-mass frame.

The differential cross section for this process is described in terms of five kinematic variables. These may be, for instance, two Lorentz invariants and three angles. One obvious choice for one of the invariants is $s$. The choice of the other four quantities can be fairly arbitrary, and depends on what information is being presented. One choice is the scattering angle of the nucleon, $\theta$, or equivalently, $t$. For the other three variables, we can choose, for example, $s_{K\bar{K}} \equiv (q_1 + q_2)^2$ and $d\Omega^*_{K\bar{K}} \equiv d\Theta^*_{K\bar{K}} d\Phi^*_{K\bar{K}}$. Here, $\Theta^*_{K\bar{K}}$ and $\Phi^*_{K\bar{K}}$ are determined in the rest frame of the $K\bar{K}$ pair, relative to a $z'$ axis defined by the direction of motion of the pair of kaons. Another equally valid choice would be $s_{NK} \equiv (p_2 + q_1)^2$ and $d\Omega^*_{NK}$, where the solid angle is defined in the rest frame of the nucleon-kaon pair.

The differential cross section is

$$\frac{\partial \sigma}{\partial M^2_{NK} \partial M^2_{N\bar{K}}} = \frac{1}{(2\pi)^5} \frac{1}{p_1 \cdot k} \int \overline{|M|^2} d\cos\theta d\Phi^*_{K\bar{K}}, \quad (2)$$

where $\theta$ is the scattering angle of the $K\bar{K}$ pair relative to the momentum of the incident photon, in the rest frame of the initial photon and nucleon.

### B. General amplitude

Our starting point is the construction of the most general form for the transition amplitude for this process. While the requirements of Lorentz covariance and gauge invariance delimit the form of the amplitude, we find that there is nevertheless quite a bit of freedom in the form chosen. The most general form is

$$i\mathcal{M} = \overline{U(p_2)} \varepsilon_\mu \mathcal{O}^\mu U(p_1), \quad (3)$$

where

$$\mathcal{O}^\mu = a_1 p_1^\mu + a_2 p_2^\mu + a_3 q_1^\mu + a_4 \gamma^\mu + \not{k}(a_5 p_1^\mu + a_6 p_2^\mu + a_7 q_1^\mu$$
$$+ a_8 \gamma^\mu) + \not{q}_1(a_9 p_1^\mu + a_{10} p_2^\mu + a_{11} q_1^\mu + a_{12} \gamma^\mu)$$
$$+ \not{q}_1 \not{k}(a_{13} p_1^\mu + a_{14} p_2^\mu + a_{15} q_1^\mu + a_{16} \gamma^\mu). \quad (4)$$

Note that we have no terms in $\not{p}_1$ nor $\not{p}_2$, as the initial and final nucleons each satisfy

$$\not{p}U(p) = mU(p). \quad (5)$$

The amplitude coefficients $a_i$ are all functions of the kinematic variables $s$, $s_{K\bar{K}}$, $\theta$, $\Theta^*$, and $\Phi^*$, or whatever combination of kinematic variables is chosen. Their exact dependence on each of these variables will be determined by the specific model constructed.

Gauge invariance of the amplitude requires that $k_\mu \mathcal{O}^\mu = 0$, which leads to the four relations

$$a_1 k \cdot p_1 + a_2 k \cdot p_2 + a_3 q_1 \cdot k = 0, \quad (6)$$

$$a_4 + a_5 k \cdot p_1 + a_6 k \cdot p_2 + a_7 q_1 \cdot k = 0, \quad (7)$$

$$a_9 k \cdot p_1 + a_{10} k \cdot p_2 + a_{11} q_1 \cdot k = 0, \tag{8}$$

$$a_{12} + a_{13} k \cdot p_1 + a_{14} k \cdot p_2 + a_{15} q_1 \cdot k = 0. \tag{9}$$

Note that there is no condition on either $a_8$ or $a_{16}$.

From these equations, we can eliminate four of the amplitude coefficients, leaving us with 12 independent ones, or Lorentz-Dirac structures, to describe the amplitude. One choice would be to eliminate $a_1$, $a_4$, $a_9$, $a_{12}$, which gives

$$\varepsilon_\mu \mathcal{O}^\mu = \left\{ \frac{1}{p_1 \cdot k} [(a_2 + a_{10}\slashed{q}_1)p_{2\mu}p_{1\nu} + (a_3 + a_{11}\slashed{q}_1)p_{2\mu}p_{1\nu}] \right.$$
$$+ (a_5 + a_{13}\slashed{q}_1)p_{1\nu}\gamma_\mu + (a_6 + a_{14}\slashed{q}_1)p_{2\mu}\gamma_\nu$$
$$\left. + (a_7 + a_{15}\slashed{q}_1)q_{1\mu}\gamma_\nu - \frac{1}{2}(a_8 + a_{16}\slashed{q}_1)\gamma_\mu\gamma_\nu \right\} F^{\mu\nu},$$

where $F^{\mu\nu} = \varepsilon^\mu k^\nu - \varepsilon^\nu k^\mu$. Another choice is $a_1$, $a_5$, $a_9$, $a_{13}$, giving

$$\varepsilon_\mu \mathcal{O}^\mu = \left\{ \frac{1}{p_1 \cdot k} [(a_2 + \slashed{k}a_6 + \slashed{q}_1 a_{10} + \slashed{q}_1\slashed{k}a_{14})p_{2\mu}p_{1\nu} \right.$$
$$+ (a_4 + \slashed{q}_1 a_{12})p_{1\nu}\gamma_\mu + (a_3 + \slashed{k}a_7 + \slashed{q}_1 a_{11}$$
$$\left. + \slashed{q}_1\slashed{k}a_{15})q_{1\mu}p_{1\nu}] - \frac{1}{2}(a_8 + a_{16}\slashed{q}_1)\gamma_\mu\gamma_\nu \right\} F^{\mu\nu}.$$

Note that these two forms contain a potential kinematic singularity at $p_1 \cdot k = 0$. However, this singularity is outside the physically accessible region for the process we are discussing, and since this calculation involves no loop integrations, such singularities are of no real concern.

A further four structures may be eliminated by use of so-called equivalence relations, leaving a total of eight. A more detailed discussion of this is beyond the scope of this paper.

## III. PHENOMENOLOGICAL LAGRANGIANS

The framework in which we treat the process $\gamma N \to NK\bar{K}$ is the phenomenological Lagrangian. In this approach, all particles are treated as pointlike. Their structure is accounted for by inclusion of phenomenological form factors, which we discuss in a later subsection.

### A. Ground-state baryons

We begin with the Lagrangians needed for the electromagnetic vertices of pseudoscalar mesons and ground-state baryons. We treat nucleons as an isospin doublet, with

$$N = \begin{pmatrix} p \\ n \end{pmatrix}.$$

Kaons are also treated as isospin doublets

$$\left[ K = \begin{pmatrix} K^+ \\ K^0 \end{pmatrix} \right].$$

$\pi$ and $\Sigma$ are treated as isotriplets.

In what should be a transparent notation, the electromagnetic part of the Lagrangian is (omitting the $\Theta^+$ for the time being)

$$\mathcal{L}_1 = \bar{N}\left( -\frac{e}{2}(1 + \tau_3)\gamma_\mu A^\mu + \frac{e}{4M_N}(k_s^N + \tau_3 k_v^N)\gamma_\mu\gamma_\nu F^{\mu\nu} \right)N + \bar{\Sigma}\left( -\frac{e}{2}(1 + T_3)\gamma_\mu A^\mu + \frac{e}{4M_\Sigma}(k_s^\Sigma + \tau_3 k_v^\Sigma)\gamma_\mu\gamma_\nu F^{\mu\nu} \right)\Sigma$$

$$+ \bar{\Lambda}\frac{e}{4M_\Lambda}\mu_\Lambda\gamma_\mu\gamma_\nu F^{\mu\nu}\Lambda + \bar{\Sigma}^0\frac{e}{2(M_\Sigma^0 + M_\Lambda)}\mu_{\Sigma\Lambda}\gamma_\mu\gamma_\nu F^{\mu\nu}\Lambda - \frac{e}{2}[K^\dagger(1 + \tau_3)(\partial_\mu K) - (\partial_\mu K^\dagger)(1 + \tau_3)K]A^\mu + \text{H.c.}, \tag{10}$$

where $\mu_{\Sigma\Lambda}$ is the $\Sigma^0 \to \Lambda$ transition magnetic moment, $\mu_\Lambda$ is the magnetic moment of the $\Lambda$, $k_s^N$ and $k_v^N$ describe the anomalous magnetic moments of the nucleon doublet, and the $k_{s,v}^\Sigma$ are the corresponding quantities for the $\Sigma$ isotriplet. $T_3$ is the isospin operator for the isotriplet.

The coupling of pseudoscalar mesons to ground-state baryons is described by the Lagrangian

$$\mathcal{L}_2 = \frac{g_{NN\pi}}{2M_N}\bar{N}\gamma_\mu\gamma_5(\partial^\mu\pi \cdot \tau)N + \frac{g_{N\Lambda K}}{M_N + M_\Lambda}\bar{N}\gamma_\mu\gamma_5(\partial^\mu K)\Lambda + \frac{g_{N\Sigma K}}{M_N + M_\Sigma}\bar{N}\gamma_\mu\gamma_5\Sigma \cdot \tau\partial^\mu K + \frac{g_{NN\eta}}{2M_N}\bar{N}\gamma_\mu\gamma_5 N(\partial^\mu\eta)$$

$$- e\frac{g_{NN\pi}}{2M_N}\bar{N}\gamma_\mu\gamma_5 A^\mu\tau_3\pi \cdot \tau N - e\frac{g_{N\Lambda K}}{M_N + M_\Lambda}\bar{N}\gamma_\mu\gamma_5 A^\mu\tau_3 K\Lambda - e\frac{g_{N\Sigma K}}{M_N + M_\Sigma}\bar{N}\gamma_\mu\gamma_5\Sigma \cdot \tau A^\mu\tau_3 K + \text{H.c.} \tag{11}$$

$\eta$ is an isosinglet field representing the $\eta$ meson. The last three terms of this Lagrangian are obtained by minimal substitution in the first three terms.

### B. Vector mesons

The vector mesons that enter into our model are $K^*$ and $\phi$. The $K^*$ is treated as a vector isodoublet field $K_\mu$, completely analogously to the $K$, while the $\phi$ is represented by a vector isosinglet field $\phi_\mu$. The Lagrangian in this sector is

$$\mathcal{L}_3 = \bar{N}\left( G_v^\phi \gamma^\mu \phi_\mu + i\frac{G_t^\phi}{2M_N}\gamma^\mu \gamma^\nu(\partial_\nu \phi_\mu)\right)N + \bar{N}\left( G_v^{K^*N\Lambda}\gamma^\mu K_\mu^* + i\frac{G_t^{K^*N\Lambda}}{M_N+M_\Lambda}\gamma^\mu \gamma^\nu(\partial_\nu K_\mu^*)\right)\Lambda + \bar{N}\left( G_v^{K^*N\Sigma}\gamma^\mu \Sigma \cdot \tau K_\mu^* \right.$$

$$+ i\frac{G_t^{K^*N\Sigma}}{M_N+M_\Sigma}\gamma^\mu \gamma^\nu \Sigma \cdot \tau \partial_\nu K_\mu^* \Bigg) + \epsilon^{\alpha\beta\mu\nu}\left( \frac{g_{\phi\pi\gamma}}{m_\pi}\phi_\alpha(\partial_\mu A_\beta)\partial_\nu\pi^0 + \frac{g_{\phi\eta\gamma}}{m_\eta}\phi_\alpha(\partial_\mu A_\beta)\partial_\nu\eta \right) + \frac{g_{\phi KK}}{m_K}[K^\dagger(\partial^\mu K) - (\partial^\mu K^\dagger)K]\phi_\mu$$

$$+ \frac{g_{K^*K\pi}}{m_K}[K^\dagger(\partial^\mu \pi \cdot \tau) - (\partial^\mu K^\dagger)\pi \cdot \tau]K_\mu^*. \tag{12}$$

### C. Baryon resonances

There are a number of resonances that need to be taken into account in a calculation such as this. Since the experimental target is a nucleon, any of the nucleon or $\Delta$ resonances are expected to play a role. For the energy range that we consider, and more particularly, for the scope of this calculation, we find that the most salient points can be illustrated without any nonstrange resonances. Among the hyperons, any number of them can be included, but again we limit the scope so that only the lowest few hyperon resonances are taken into account. In either case, we do not consider any baryon with spin greater than $3/2$. With the scope of the model limited like this, there are only a few Lagrangian terms that must be considered in this sector. The nonexotic hyperons that are included are listed in Table II.

### 1. Spin 1/2

Lagrangian terms needed for spin-$1/2$ resonances are

$$\mathcal{L}_4 = \bar{N}\frac{g_{\Sigma^*NK}^{(1/2)}}{m_K}\gamma_\mu\gamma_5\Sigma^* \cdot \tau\partial^\mu K + \bar{N}\frac{g_{\Lambda^*NK}^{(1/2)}}{m_K}\gamma_\mu\gamma_5(\partial^\mu K)\Lambda^*$$

$$+ \bar{N}\frac{g_{\Theta NK}^{(1/2)}}{m_K}\gamma_\mu\gamma_5(\partial^\mu K)\Theta_+ + \bar{N}\frac{g_{\Sigma^*NK}^{(1/2)}}{m_K}\gamma_\mu\Sigma^* \cdot \tau\partial^\mu K$$

$$+ \bar{N}\frac{g_{\Lambda^*NK}^{(1/2)}}{m_K}\gamma_\mu(\partial^\mu K)\Lambda^* + \bar{N}\frac{g_{\Theta NK}^{(1/2)}}{m_K}\gamma_\mu(\partial^\mu K)\Theta_- + \text{H.c.},$$

$$\tag{13}$$

where $\Theta_\pm$ is the field for $\Theta^+$ with $J^P=1/2^\pm$. The first three terms of this Lagrangian correspond to states with $J^P=1/2^+$, while the last three terms are for $J^P=1/2^-$. In addition, the $\Theta^+$ part of the Lagrangian written above assumes that the state is an isosinglet. For an isotriplet $\Theta^+$ with $J^P=1/2^+$, the Lagrangian would become

$$\mathcal{L}_5 = \bar{N}\frac{g_{\Theta NK}}{m_K}\gamma_\mu\gamma_5\Theta_+ \cdot \tau\partial^\mu K + \bar{N}\frac{g_{\Theta NK}}{m_K}\gamma_\mu\Theta_- \cdot \tau\partial^\mu K.$$

$$\tag{14}$$

### 2. Spin 3/2

The Lagrangian terms for spin-$3/2$ resonances are

$$\mathcal{L}_6 = \bar{N}\frac{g_{\Sigma^*NK}^{(3/2)}}{m_K}\Sigma_\mu^* \cdot \tau\partial^\mu K + \bar{N}\frac{g_{\Lambda^*NK}^{(3/2)}}{m_K}(\partial^\mu K)\Lambda_\mu^*$$

$$+ \bar{N}\frac{g_{\Theta NK}^{(3/2)}}{m_K}(\partial^\mu K)\Theta_{+\mu}$$

$$+ \bar{N}\frac{g_{\Sigma^*NK}^{(3/2)}}{m_K}\gamma_5\Sigma_\mu^* \cdot \tau\partial^\mu K + \bar{N}\frac{g_{\Lambda^*NK}^{(3/2)}}{m_K}\gamma_5(\partial^\mu K)\Lambda_\mu^*$$

$$+ \bar{N}\frac{g_{\Theta NK}^{(3/2)}}{m_K}\gamma_5(\partial^\mu K)\Theta_{-\mu} + \text{H.c.}, \tag{15}$$

where the $\mu$ indices on the $\Lambda$, $\Sigma$, and $\Theta$ fields indicate that they are vector-spinor, spin-$3/2$ fields. In this calculation, we use the Rarita-Schwinger version of such fields. The first three terms are for resonances with positive parity, while the last three are for resonances with negative parity. For an isovector $\Theta$, the Lagrangian terms are

$$\mathcal{L}_7 = \bar{N}\frac{g_{\Theta NK}}{m_K}\Theta_{+\mu} \cdot \tau\partial^\mu K + i\bar{N}\frac{g_{\Theta NK}}{m_K}\gamma_5\Theta_{-\mu} \cdot \tau\partial^\mu K, \tag{16}$$

where the $\Theta_{\pm\mu}$ represents a $\Theta^+$ with $J^P=3/2^\pm$, respectively.

### D. Coupling constants

To evaluate the coupling constants of the ground-state baryons to pseudoscalar mesons, we use the extended Goldberger-Treiman relations. For the coupling of the baryons $B$ and $B'$ to the pseudoscalar $M$, the relation is

$$g_{BB'M} = \left(\frac{G_A}{G_V}\right)_{B\to B'}\frac{M_B+M_{B'}}{2f_M}, \tag{17}$$

where $f_M$ is the meson decay constant for the pseudoscalar meson $M$. $(G_A/G_V)_{B\to B'}$ is obtained from the semileptonic decay of $B\to B'$ or $B'\to B$. The values of $f_M$, $(G_A/G_V)_{B\to B'}$ (taken from the *Review of Particle Physics* [50]), and $g_{BB'M}$ obtained from these relations are shown in Table I.

The decay width of a vector meson into two pseudoscalars is related to the corresponding coupling constant by

$$\Gamma_{V\to P_1P_2} = \frac{g_{VP_1P_2}^2}{48\pi M_V^5}\lambda^{3/2}(M_V^2, M_{P_1}^2, M_{P_2}^2), \tag{18}$$

where $\lambda(a,b,c)$ is the Källen function $\lambda(a,b,c)=a^2+b^2+c^2-2(ab+ac+bc)$. From the measured widths and branch-

TABLE I. Values of $g_{BB'M}$ obtained using the Goldberger-Treimann relations.

| Coupling | $f_M$ (GeV) | $(G_A/G_V)_{B\to B'}$ | $g_{BB'M}$ |
|---|---|---|---|
| $g_{\pi NN\pi}$ | $0.13/\sqrt{2}$ | 1.22 | 12.8 |
| $g_{N\Sigma K}$ | $0.16/\sqrt{2}$ | 0.34 | 3.2 |
| $g_{N\Lambda K}$ | $0.16/\sqrt{2}$ | $-0.718$ | $-6.51$ |
| $g_{NN\eta}$ | $\approx 1.2 f_\pi$ | 1.22 | 10.37 |

ing fractions of the $\phi$ and $K^*$ mesons, we find that

$$g_{\phi KK} = 4.3, g_{K^*K\pi} = 5.6. \qquad (19)$$

In a similar way, the width for the process $V \to P\gamma$ is

$$\Gamma_{V\to P\gamma} = \frac{g_{VP\gamma}^2}{192\pi M_V^3}\lambda^{3/2}(M_V^2, M_P^2, 0), \qquad (20)$$

which leads to

$$g_{\phi\eta\gamma} = 4.3, g_{\phi\pi^0\gamma} = 0.055, g_{K^{0*}K^0\gamma} = 0.35, g_{K^{+*}K^+\gamma} = 0.22. \qquad (21)$$

For a baryon $B$ with $J^P = 1/2^+$, the width for the decay into a pseudoscalar meson $P$ and a ground-state baryon $B'$ is

$$\Gamma_{B\to B'P} = \frac{g_{BB'P}^2}{16\pi M_B^3 M_P^2}(M_B + M_{B'})^2[(M_B - M_{B'})^2 - M_P^2] \\ \times \lambda^{1/2}(M_B^2, M_{B'}^2, M_P^2), \qquad (22)$$

while the corresponding width for a baryon with $J^P = 1/2^-$ is

TABLE II. Values of $g_{YNK}$ for nonexotic hyperons appearing in the model.

| $Y$ (Mass) | $J^P$ | $\Gamma$(MeV) | $\dot{\Gamma}_{NK}/\Gamma$ | $g_{YNK}$ |
|---|---|---|---|---|
| $\Lambda(1520)$ | $\frac{3}{2}^-$ | 16 | 0.45 | 15.2 |
| $\Lambda(1600)$ | $\frac{1}{2}^+$ | 150 | 0.2 | 1.05 |
| $\Lambda(1670)$ | $\frac{1}{2}^-$ | 35 | 0.25 | 0.32 |
| $\Lambda(1690)$ | $\frac{3}{2}^-$ | 60 | 0.25 | 5.53 |
| $\Lambda(1800)$ | $\frac{1}{2}^+$ | 300 | 0.35 | 0.86 |
| $\Lambda(1810)$ | $\frac{1}{2}^+$ | 150 | 0.35 | 0.71 |
| $\Lambda(1890)$ | $\frac{3}{2}^+$ | 100 | 0.3 | 1.09 |
| $\Sigma(1580)$ | $\frac{3}{2}^-$ | 15 | 0.45 | 1.95 |
| $\Sigma(1620)$ | $\frac{1}{2}^-$ | 80 | 0.22 | 0.52 |
| $\Sigma(1660)$ | $\frac{1}{2}^+$ | 100 | 0.2 | 0.67 |
| $\Sigma(1670)$ | $\frac{3}{2}^-$ | 60 | 0.1 | 3.88 |
| $\Sigma(1750)$ | $\frac{1}{2}^-$ | 90 | 0.26 | 0.44 |
| $\Sigma(1880)$ | $\frac{1}{2}^+$ | 80 | 0.06 | 0.19 |
| $\Sigma(1940)$ | $\frac{3}{2}^-$ | 220 | 0.13 | 3.19 |

TABLE III. Values of $g_{\Theta NK}$ for different spins, parities, and total widths of the $\Theta$.

| $J$ | $P$ | $\Gamma$ (MeV) | $g_{\Theta NK}$ |
|---|---|---|---|
| $\frac{1}{2}$ | $+$ | 1 | 0.27 |
| $\frac{1}{2}$ | $+$ | 10 | 0.87 |
| $\frac{1}{2}$ | $-$ | 1 | 0.16 |
| $\frac{1}{2}$ | $-$ | 10 | 0.50 |
| $\frac{3}{2}$ | $+$ | 1 | 0.61 |
| $\frac{3}{2}$ | $+$ | 10 | 1.94 |
| $\frac{3}{2}$ | $-$ | 1 | 4.35 |
| $\frac{3}{2}$ | $-$ | 10 | 13.76 |

$$\Gamma_{B\to B'P} = \frac{g_{BB'P}^2}{16\pi M_B^3 M_P^2}(M_B - M_{B'})^2[(M_B + M_{B'})^2 - M_P^2] \\ \times \lambda^{1/2}(M_B^2, M_{B'}^2, M_P^2). \qquad (23)$$

For baryons with $J^P = 3/2^\pm$, the widths are

$$\Gamma_{B\to B'P} = \frac{g_{BB'P}^2}{192\pi M_B^5 M_P^2}[(M_B + M_{B'})^2 - M_P^2] \\ \times \lambda^{3/2}(M_B^2, M_{B'}^2, M_P^2),$$

$$\Gamma_{B\to B'P} = \frac{g_{BB'P}^2}{192\pi M_B^5 M_P^2}\frac{\lambda^{5/2}(M_B^2, M_{B'}^2, M_P^2)}{[(M_B + M_{B'})^2 - M_P^2]}, \qquad (24)$$

where the first expression is for a positive-parity parent baryon. The nonexotic hyperons that are used in this calculation, along with their masses, total widths, spins, parities, and their $NK$ branching fractions and coupling constants, obtained from Eqs. (22)–(24), are shown in Table II.

As mentioned above, we allow the $\Theta$ pentaquarks to have four different combinations of spin and parity in this calculation. In addition, since the width of this particle has not yet been ascertained, we also allow different widths. Table III shows the values of the coupling constants we obtain for the different spins, parities, and total widths of the $\Theta$, assuming that the $NK$ final state saturates its decays.

Finally, we note that there are a number of coupling constants for which little information is available. Perhaps the most important of these in terms of contributions to the cross sections are the couplings of the vector mesons $K^*$ and $\phi$, particularly those of the $\phi$ to the ground-state baryons. The couplings of the two hyperon resonances that lie below the $NK$ threshold, namely the $\Sigma(1385)$ and the $\Lambda(1405)$, are also not known with much certainty. When we display and discuss our results, we will comment further on the effects that these coupling constants have on the graphs that we show.

**E. Diagrams**

The diagrams that we include in this calculation are shown in Figs. 1–3. In these diagrams, solid lines represent baryons. If a solid line is unlabeled, it represents a nucleon.
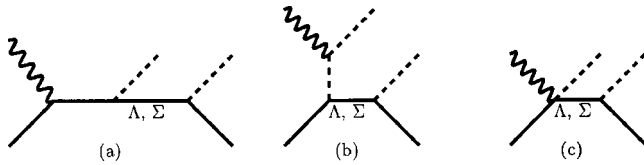
FIG. 1. "Born" diagrams: continuous, unlabeled lines are nucleons. Unlabeled dashed lines are kaons and wavy lines are photons.

Dashed lines represent pseudoscalar mesons, with unlabeled dashed lines representing kaons. Wavy lines are photons and dotted lines are vector mesons. Each diagram shown actually represents a set of diagrams, as all allowed permutations of external meson and photon legs are taken into account.

We include a number of hyperon resonances in this calculation. These are listed in Table II. For each of the resonances, there is a corresponding set of diagrams of the kind shown in Fig. 3.

There are a number of contributions that have been omitted from this calculation. For instance, we have omitted all but the ground-state nucleon, and all of the $\Delta$ resonances. In fact, with the information that is available on how these states couple to final states with hidden strangeness, we have found that their contributions to the cross section are small. We have also neglected couplings to higher moments of any of the hyperon resonances [Fig. 3(d)], as well as any contributions that would arise from electromagnetic transitions between excited hyperons and their ground states. In principle, there is no *a priori* reason to expect such contributions to be small, but little is known of those couplings. Including such contributions would add too many unknown parameters to the model.
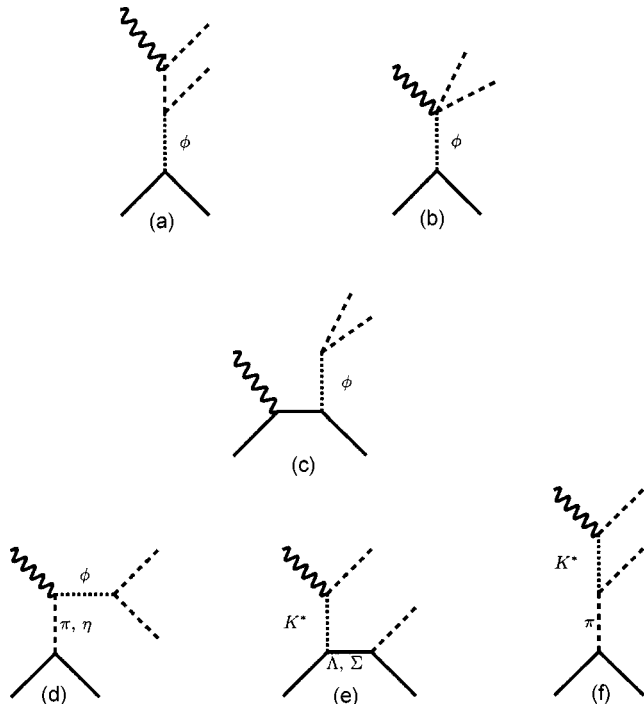


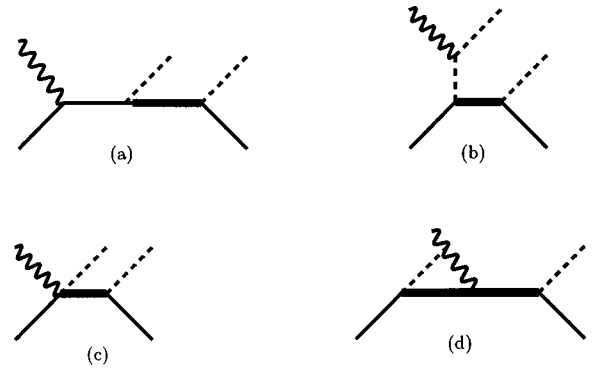FIG. 2. Diagrams containing vector mesons. The dotted lines represent the vector mesons.



FIG. 3. Diagrams containing excited baryons. In (a)–(d), the thick solid lines may be either $\Lambda^*$, $\Sigma^*$, or $\Theta$, while the thin solid line is a nucleon. In diagram (d), the photon couples to the charge of the intermediate resonance: in this model, we neglect couplings to any higher moments of the resonance.

### F. Form factors

Apart from the photon, none of the states that enter this calculation are elementary particles: they all have substructure, and this substructure is reflected in the need to include some kind of form factor at each interaction vertex. Indeed, without such form factors, cross sections grow with energy, and the unitarity limit is quickly violated.

Inclusion of any form factors in a calculation like this must be done in a manner that preserves gauge invariance, and a detailed discussion of all of the issues that arise, and all of the methods and prescriptions for preserving gauge invariance, are beyond the scope of this paper. In this calculation, we adopt the prescription of assigning an overall form factor to gauge invariant sets of diagrams. This means, for instance, that all of the diagrams of the type shown in Fig. 1 have the same form factor as a multiplicative factor. For all of the form factors, we choose the form [43,45]

$$F = \left( \frac{X^4}{(p_i^2 - m_i^2)^2 + X^4} \right)^n . \tag{25}$$

In this expression, $p_i$ is usually the momentum of the off-shell particle with mass $m_i$. In this calculation, we make the simplification of setting all of the $p_i^2$ to be equal to $s$, the total energy in the cm frame, squared. $X$ is chosen to be 1.8 GeV, as has been used by other authors. In addition, since we apply this form factor to sets of diagrams, we choose $m_i$ to be the mass of the lightest off-shell particle in a particular set. The exception to this occurs in the diagrams of Figs. 2(d) and 2(f), where $m_i$ is chosen to be the mass of the vector meson in the diagram. The value of the integer $n$ depends on the spin of baryons in the diagram. If there are only spin-1/2 baryons in the set of diagrams, $n$ is chosen to be unity, while for spin- 3/2 baryons, $n$ is chosen to be two.

The form that we have chosen for the form factors, as well as the manner in which we apply them, is simply a prescription, and is not meant to be rigorous. We note that the form factors chosen have the desired effect, producing cross sections that are roughly of the correct order of mag-

nitude. Without these form factors, calculated cross sections are much too large.

## IV. RESULTS

There are six possible channels to be explored, namely $\gamma p \rightarrow p K^+ K^-$, $\gamma p \rightarrow p K^0 \bar{K}^0$, $\gamma p \rightarrow n K^+ \bar{K}^0$, $\gamma n \rightarrow n K^+ K^-$, $\gamma n \rightarrow n K^0 \bar{K}^0$, and $\gamma n \rightarrow p K^0 K^-$. It will be impossible to present results for all of these channels without making this paper overly long. We therefore choose a few examples to illustrate the main features of the model. We note, however, that the first result reported from JLab used a deuteron target, while searches using proton targets have been and are being carried out. Examining the cross sections for both kinds of targets is therefore relevant.

In the following subsections, we present the results of our model calculation. We begin with the results of the full model, including the $\phi$ and $\Lambda(1520)$. We then exclude these two states to more closely simulate the pentaquark searches that have been carried out at JLab, and examine the effects of the spin, parity, width, and isospin of the pentaquark on the cross section. We also examine the role of the $K^*$ in increasing the cross section for production of the $\Theta^+$.

We note that the $\Sigma(1385)$ plays very little role in the results we present, as its contribution to the cross section is small. The same is true of the $N^*$ states that we consider, as their couplings to $\Lambda K$ and $\Sigma K$ final states are generally small, at least for the ones we have examined. The $\Lambda(1405)$, on the other hand, can significantly affect the cross section near threshold in the $N\bar{K}$ mass distributions. If the value for the coupling of this state to the $N\bar{K}$ channel is chosen to be sufficiently large, a sharp shoulder at lower masses arises in the mass distribution of the $N\bar{K}$. The absence of such a shoulder in the experimental data limits the size of this coupling constant. We use a value of 5.3 for this constant.

In Ref. [3], the process studied was $\gamma d \rightarrow p n K^+ K^-$. The $\Lambda(1520)$ was identified in the mass distribution of the $pK^-$ pair, the $\phi$ in the $K^+ K^-$ pair, and the $\Theta^+$ in the $nK^+$ pair. We assume that either one of the initial nucleons takes an active part in the scattering process, while the other acts as a spectator. This would mean that the two processes contributing to the $pnK^+K^-$ final state are $\gamma p \rightarrow p K^+ K^-$ and $\gamma n \rightarrow n K^+ K^-$. In addition, this means that in the mass distributions observed, only the proton component of the target contributes to the production of the $\Lambda(1520)$, and only the neutron component contributes to the production of the isoscalar $\Theta^+$. The two processes $\gamma p \rightarrow p K^+ K^-$ and $\gamma n \rightarrow n K^+ K^-$ are therefore the focus of much of our discussion. However, searches in other channels have been and are being carried out, and some discussion is devoted to those channels as well.

### A. Full model

For all of the results that we display, we present $\partial\sigma/\partial m_{ij}^2$, where $m_{ij}^2 = (p_i + p_j)^2$, and $p_i$ is the momentum of the $i$th particle in the final state. Thus, we expect to see strong resonant effects from the $\phi$ in the $K\bar{K}$ subsystem, and similar effects arising from the $\Lambda(1520)$ in the $N\bar{K}$ subsystem. We also ex-
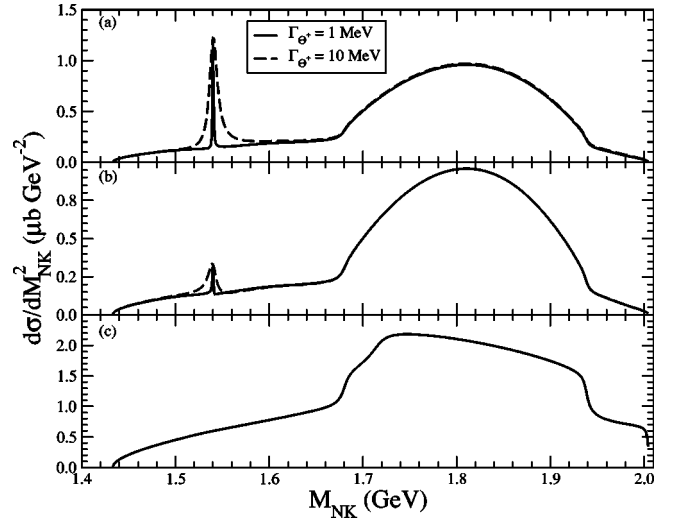


FIG. 4. The differential cross section $\partial\sigma/\partial M_{NK}^2$ as a function of $M_{NK}$, for a spin-1/2 $\Theta^+$. The curves in (a) and (b) are for the process $\gamma n \rightarrow n K^+ K^-$, while the curve in (c) is for $\gamma p \rightarrow p K^+ K^-$. In (a) and (b), the solid curves arise for a pentaquark with a width of 1 MeV, while the dashed curves correspond to a width of 10 MeV. The curves in (a) arise from a pentaquark with positive parity, while those in (b) are for a pentaquark of negative parity.

pect to see weaker resonant effects from the other hyperons that are included in the calculation.

While the coupling of the $\Lambda(1520)$ to $NK$ can be determined from the $NK$ partial width of the state, there is no simple way of determining the $\phi NN$ coupling constants, except by a detailed analysis of $\phi$ photoproduction cross sections. Indeed, the angular distributions would have to be analyzed in order to determine the relative magnitudes and signs of the vector and tensor couplings. Such an analysis is well beyond the scope of this work. In the results that we show for the full calculation, we choose $G_v^\phi = 4$ and $G_t^\phi = 5$. The actual values are of no import for the main topic of the paper. We must also point out that we have not included any diffractive production of the $\phi$.

The results that we show are for $w = 2.5$ GeV. We have examined some of the cross sections for smaller values of $w$, and we will comment on those results later in the paper.

#### 1. Isoscalar, spin-1/2 $\Theta^+$

Figure 4 shows the differential cross section, $\partial\sigma/\partial M_{NK}^2$, for an isoscalar $\Theta^+$ with spin 1/2. The curves in (a) and (b) are for the process $\gamma n \rightarrow n K^+ K^-$, while (c) is for $\gamma p \rightarrow p K^+ K^-$. In (a) and (b), the width of the $\Theta^+$ is allowed to be 1 MeV (solid curves) or 10 MeV (dashed curves). In addition, (a) results from a $\Theta^+$ with positive parity, while (b) corresponds to one with negative parity. Since the isoscalar $\Theta^+$ is not produced off the proton in this channel, neither its parity nor its width affects the curve that results in (c). The structures seen in this plot arise from kinematic reflections of the $\Lambda(1520)$ and the $\phi$.

If there were free neutron targets, the curves in (a) suggest that the $\Theta^+$ would be relatively easy to observe above background, modulo detector efficiency, resolution, and accep-
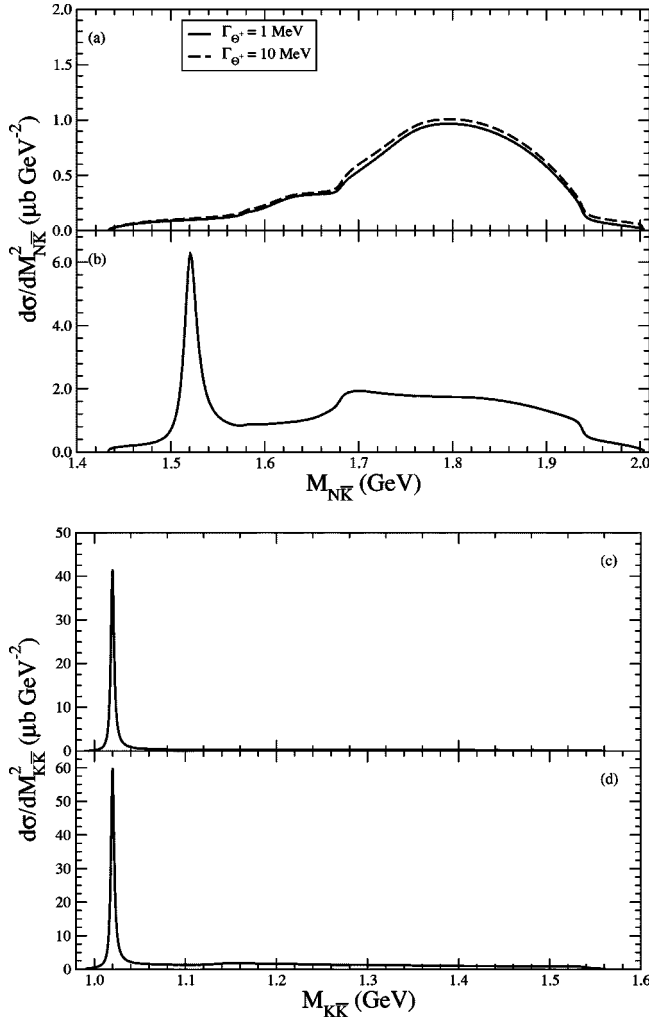
FIG. 5. The differential cross section $\partial\sigma/\partial M^2_{N\bar{K}}$ as a function of $M_{N\bar{K}}$ [(a) and (b)], and $\partial\sigma/\partial M^2_{K\bar{K}}$ as a function of $M_{K\bar{K}}$ [(c) and (d)]. The curves in (a) and (c) are for the process $\gamma n \rightarrow nK^+K^-$, while those in (b) and (d) are for $\gamma p \rightarrow pK^+K^-$.

tance issues. However, for deuteron targets, the presence of the proton would modify this somewhat.

Figure 5 shows the same differential cross sections, but as functions of different invariant masses. Figures 5(a) and 5(b) show the differential cross sections as a function of the mass of the nucleon-antikaon pair, while Figs. 5(c) and 5(d) show it as a function of the mass of the $K\bar{K}$ pair. In addition, (a) and (c) result from a neutron target, while (b) and (d) are from a proton. In the case of the proton target, the $\Lambda(1520)$ dominates the cross section in (b), while the contribution of the $\phi$ can be seen as the structure at larger values of $M_{N\bar{K}}$. The roles are reversed in (d): the $\phi$ gives the prominent peak, while the $\Lambda(1520)$ provides the "plateau" at larger invariant mass. For the neutron target [(a) and (c)], $\Lambda$'s do not contribute to this channel, but the effects of the $\Sigma$ resonances included in the calculation can be seen in (a). In this case, the bulk of the cross section comes from the $\phi$, as can be seen from (c).

Figure 6 shows the differential cross section, $\partial\sigma/\partial M^2_{N K}$, for the processes $\gamma p \rightarrow pK^0\bar{K}^0$ [(a) and (c)] and $\gamma p \rightarrow nK^+\bar{K}^0$
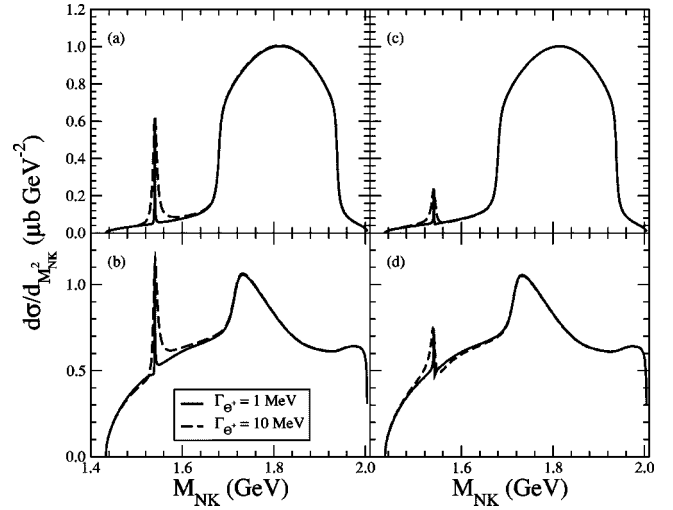


FIG. 6. The differential cross section $\partial\sigma/\partial M^2_{NK}$ as a function of $M_{NK}$. The curves in (a) and (c) are for the process $\gamma p \rightarrow pK^0\bar{K}^0$, while those in (b) and (d) are for $\gamma p \rightarrow nK^+\bar{K}^0$. (a) and (b) are for a positive parity $\Theta^+$ while (c) and (d) are for a $\Theta^+$ with negative parity.

[(b) and (d)]. The graphs in (a) and (b) assume that the $\Theta^+$ has positive parity, while those in (c) and (d) are for a pentaquark with negative parity. From these curves, particularly those in (b) and (d), it should be clear that observing a $\Theta^+$ signal could be somewhat problematic unless the contributions from the $\Lambda(1520)$ and the $\phi$ were excluded. We discuss this in a later subsection.

### 2. Isoscalar, spin-3/2 $\Theta^+$

Figure 7 shows the differential cross section if the $\Theta^+$ is assumed to be an isoscalar with spin 3/2. As with the spin-1/2 discussion, the curves in (a) and (b) are for the process
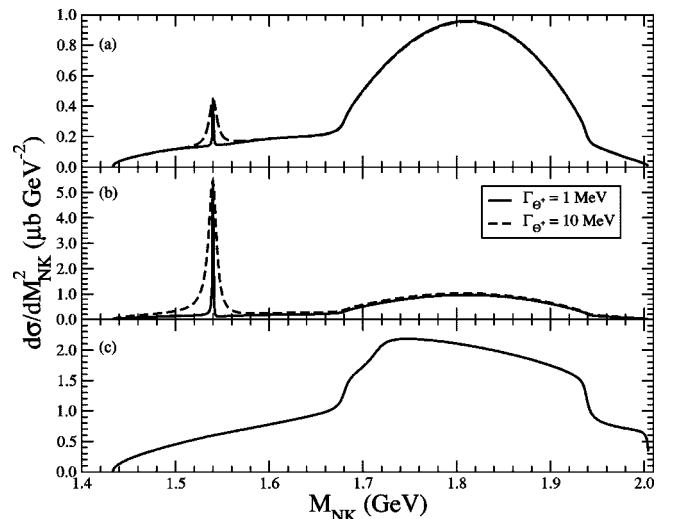


FIG. 7. The differential cross section $\partial\sigma/\partial M^2_{NK}$ as a function of $M_{NK}$, for a spin-3/2 $\Theta^+$. The curves in (a) and (b) are for the process $\gamma n \rightarrow nK^+K^-$, while (c) is for $\gamma p \rightarrow pK^+K^-$. In (a), the $\Theta^+$ has positive parity, while in (b), its parity is negative.
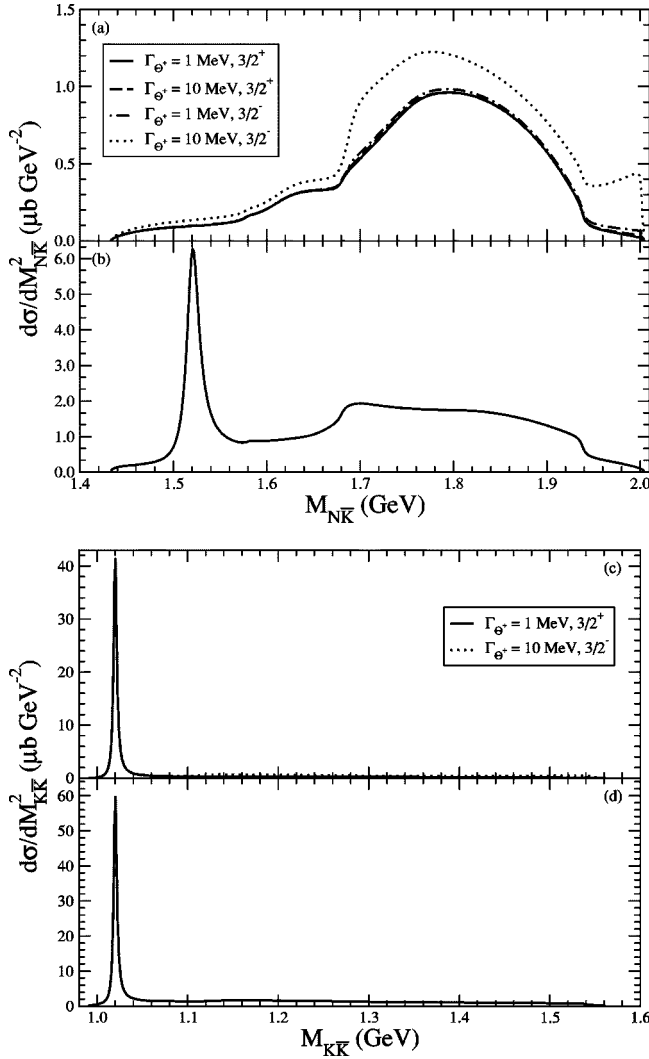
FIG. 8. The differential cross section as functions of $M_{N\bar{K}}$ [(a) and (b)] or $M_{K\bar{K}}$ [(c) and (d)]. The curves in (a) and (c) are for the process $\gamma n \rightarrow nK^+K^-$, while those in (b) and (d) are for $\gamma p \rightarrow pK^+K^-$.

$\gamma n \rightarrow nK^+K^-$, while those in (c) are for $\gamma p \rightarrow pK^+K^-$. In (a) and (b), the width of the $\Theta^+$ is allowed to be 1 MeV (solid curves) or 10 MeV (dashed curves). In addition, (a) results from a $\Theta^+$ with positive parity, while (b) corresponds to one with negative parity. It is interesting to note that the height of the peak of the $\Theta^+$ for the $3/2^-$ case is comparable to that of the $\Lambda(1520)$ [seen in Fig. 5(b), for instance]. This is not surprising, since the states are almost degenerate, and the height of the peak at resonance depends only on kinematics, which would be largely the same for the two resonances.

Figure 8 shows the same differential cross section, but as functions of different invariant masses. The curves in (a) and (b) show the differential cross sections as a function of the mass of the nucleon-antikaon pair, while the curves in (c) and (d) show it as a function of the mass of the $K\bar{K}$ pair. In each case, the upper graph results from a neutron target, while the lower graph is from a proton. Unlike the case with spin $1/2$, the contribution to the cross section of the $\Theta^+$ is now significant, especially for the negative-parity state, and gives rise to the strong kinematic reflections seen in (a), and to a lesser extent, in (c) (the dotted curves, for example).

Figure 9 shows the differential cross section for the processes $\gamma p \rightarrow pK^0\bar{K}^0$ [(a) and (c)] and $\gamma p \rightarrow nK^+\bar{K}^0$ [(b) and (d)]. The graphs on the left assume that the $\Theta^+$ has positive parity, while those on the right have negative parity. From the curves in (c) and (d), it should be clear that detecting a signal for a $\Theta^+$ with $J^P = 3/2^-$ would be relatively easy.

### 3. Isovector, spin-1/2 $\Theta^+$

If the $\Theta^+$ were an isovector, there would be a $\Theta^{++}$ state that could be seen in $K^+p$ final states, as well as a $\Theta^0$ that could be present in $nK^0$ final states. Figures 10(a) and 10(c) show the effect of such a state in $\gamma n \rightarrow nK^+K^-$, while Figs. 10(b) and 10(d) show the effect in $\gamma p \rightarrow pK^+K^-$. The curves in (a) and (b) assume that the $\Theta^+$ has positive parity, while those in (c) and (d) assume that it has negative parity. In all cases, the spin is assumed to be $1/2$. Figures 10(e) and 10(g) show the differential cross section for $\gamma p \rightarrow pK^0\bar{K}^0$, while (f)
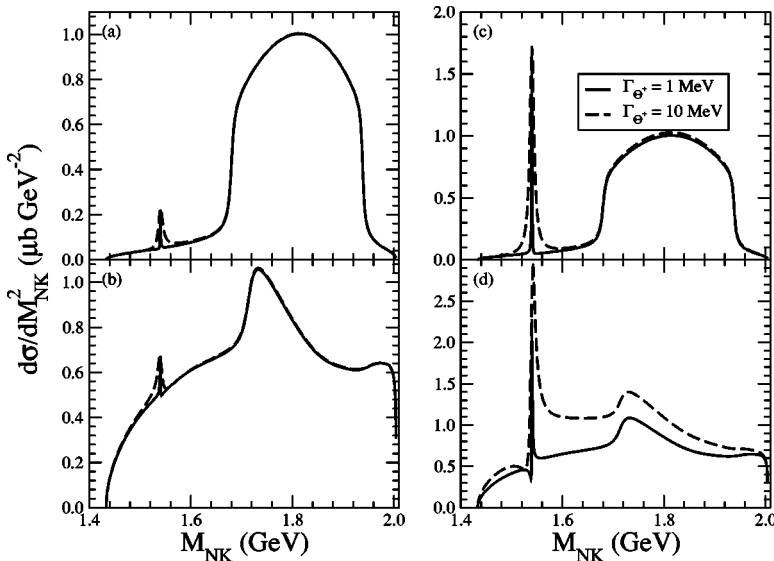


FIG. 9. The differential cross section $\partial\sigma/\partial M_{NK}^2$ as a function of $M_{NK}$. The upper graphs are for the process $\gamma p \rightarrow pK^0\bar{K}^0$, while the lower ones are for $\gamma p \rightarrow nK^+\bar{K}^0$.
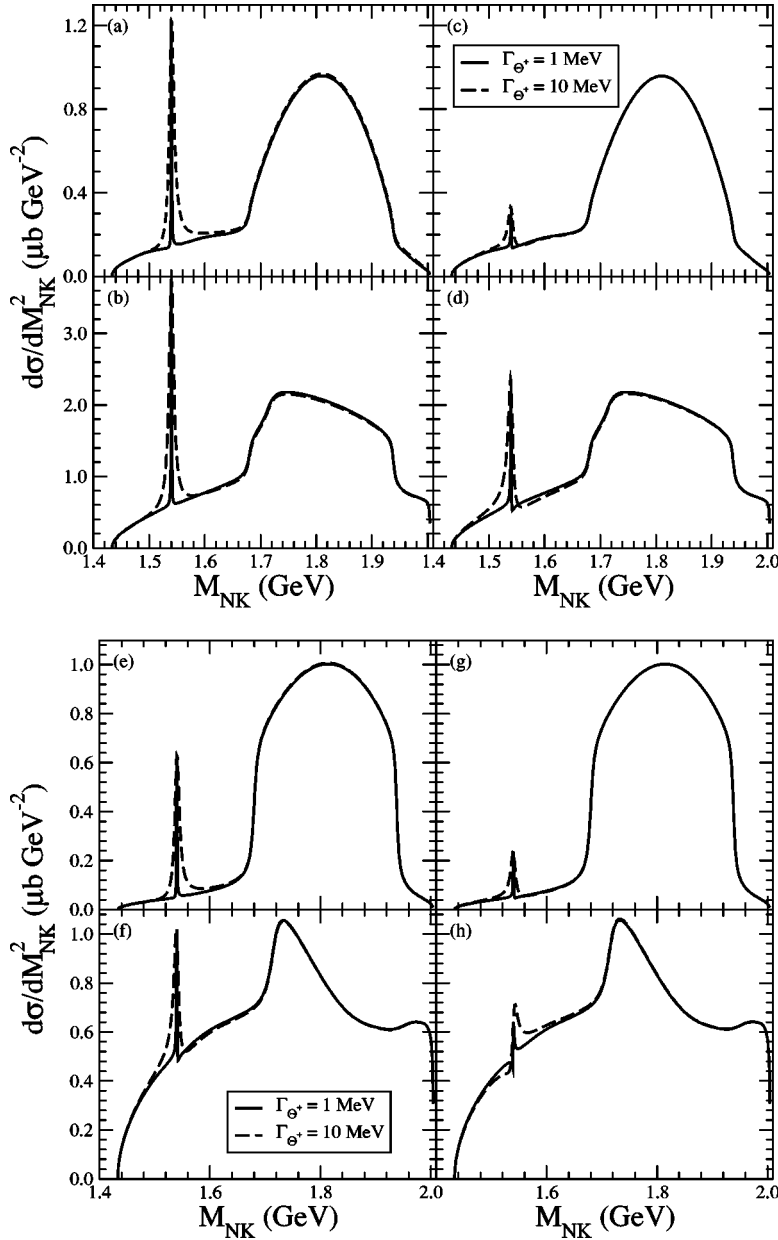
FIG. 10. The differential cross sections $\partial\sigma/\partial M^2_{NK}$ as a function of $M_{NK}$, for a spin-1/2 isovector $\Theta^+$, for the processes $\gamma n \rightarrow nK^+K^-$ [(a) and (c)], $\gamma p \rightarrow pK^+K^-$ [(b) and (d)], $\gamma p \rightarrow pK^0\bar{K}^0$ [(e) and (g)], and $\gamma p \rightarrow nK^+\bar{K}^0$ [(f) and (h)]. The curves in (a), (b), (e), and (f) all arise from a positive-parity $\Theta^+$, while those in (c), (d), (g), and (h) all correspond to a $\Theta^+$ of negative parity.

and (h) correspond to $\gamma p \rightarrow nK^+\bar{K}^0$. (e) and (f) are for a $\Theta^+$ of positive parity, while (g) and (h) assume that it has negative parity. The curves in (b) and (d) suggest that a signal for a $\Theta^{++}$ should be comparable to that for a $\Theta^+$, regardless of the parity of the state.

### B. Omitting $\Lambda(1520)$, $\phi(1020)$

It is clear from the graphs shown in the preceding discussion that the $\Lambda(1520)$ and the $\phi(1020)$ dominate the cross section for $\gamma N \rightarrow NK\bar{K}$ for most channels. To enhance the possibility of isolating a $\Theta^+$ signal, experimentalists impose kinematic cuts to eliminate the bulk of the contribution from these two states. In our case, we will simply eliminate all diagrams containing their contributions from the calculation. The curves that result are presented in the next two subsections.

We note that we could also have imposed the same kinematic cuts on the model. The (background) distributions that result when we do this are somewhat different from those that we show, but the salient points of the discussion are unchanged.

#### 1. Isoscalar, spin-1/2 $\Theta^+$

In Fig. 11, we show the differential cross section that results for a spin-1/2 $\Theta^+$, when the contributions of the $\Lambda(1520)$ and $\phi(1020)$ are omitted from the calculation. In the case of a positive-parity $\Theta^+$, a signal that may be easily identifiable results. In this figure, the smooth background is provided by the nonexotic hyperons included in the calculation. The graphs in (a) and (b) are for $\gamma n \rightarrow K^+K^-n$, while (c) is for $\gamma p \rightarrow K^+K^-p$. The curves in (a) are for a $\Theta^+$ with $J^P = 1/2^+$, while those in (b) arise from a $\Theta^+$ with $J^P = 1/2^-$.
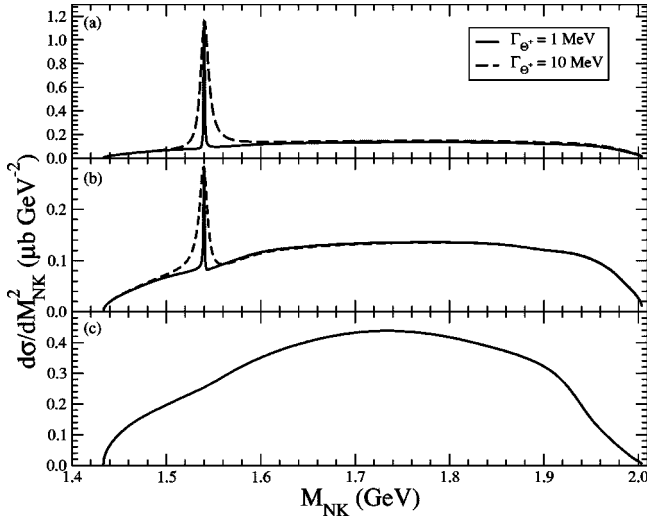
FIG. 11. The differential cross section $\partial\sigma/\partial M_{NK}^2$ as a function of $M_{NK}$, for a spin-1/2 $\Theta^+$. The curves in (a) and (b) are for the process $\gamma n \to n K^+ K^-$, while (c) is for $\gamma p \to p K^+ K^-$. In addition, (a) is for a $\Theta^+$ of positive parity, while (b) is for one of negative parity.

Figures 12(a) and 12(b) show the differential cross section as a function of the invariant mass of the $N\bar{K}$ pair. The effects of the nonexotic hyperon resonances included in the calculation can be seen in these curves. Figures 12(c) and 12(d) show the same differential cross sections as functions of the invariant mass of the $K\bar{K}$ pair. Since there are no resonances left in this channel (in this model), relatively smooth distributions with no prominent features result. In this figure, (a) and (c) are for $\gamma n \to n K^+ K^-$, while (b) and (d) are for $\gamma p \to p K^+ K^-$. The shoulder seen near threshold in (b) results from the sub-threshold $\Lambda(1405)$. If a larger coupling constant were chosen for this state, this structure would be enhanced, while choosing a sufficiently smaller value will make this feature disappear. In Fig. 13, we show the cross sections for the processes $\gamma p \to p K^0 \bar{K}^0$ [(a) and (c)] and $\gamma p \to n K^+ \bar{K}^0$ [(b) and (d)] in the channel that would show the isoscalar $\Theta^+$ resonance. The effects of the state are clearly seen, and suggest that for a pentaquark of positive parity, either channel should provide a clear signal, while for one of negative parity, the channel with two neutral kaons is better.

### 2. Isoscalar, spin-3/2 $\Theta^+$

Figure 14 shows the differential cross section for a spin-3/2 $\Theta^+$ for the processes $\gamma n \to n K^+ K^-$ [(a) and (b)] and $\gamma p \to p K^+ K^-$ [(c)]. The curves in (a) assume that the $\Theta^+$ has positive parity, while those in (b) assume negative parity. In the case of the negative-parity state, its contribution completely dominates the cross section. As mentioned before, the signal generated by such a state should be comparable to that generated by the $\Lambda(1520)$. The positive parity $\Theta^+$ also provides a large signal above the "background," although it is not as dominant as in the case of negative parity.

Figure 15 shows the same cross sections in terms of different invariant masses. In (a) and (c), the large signal from the $\Theta^+$, particularly from the negative-parity version, shows
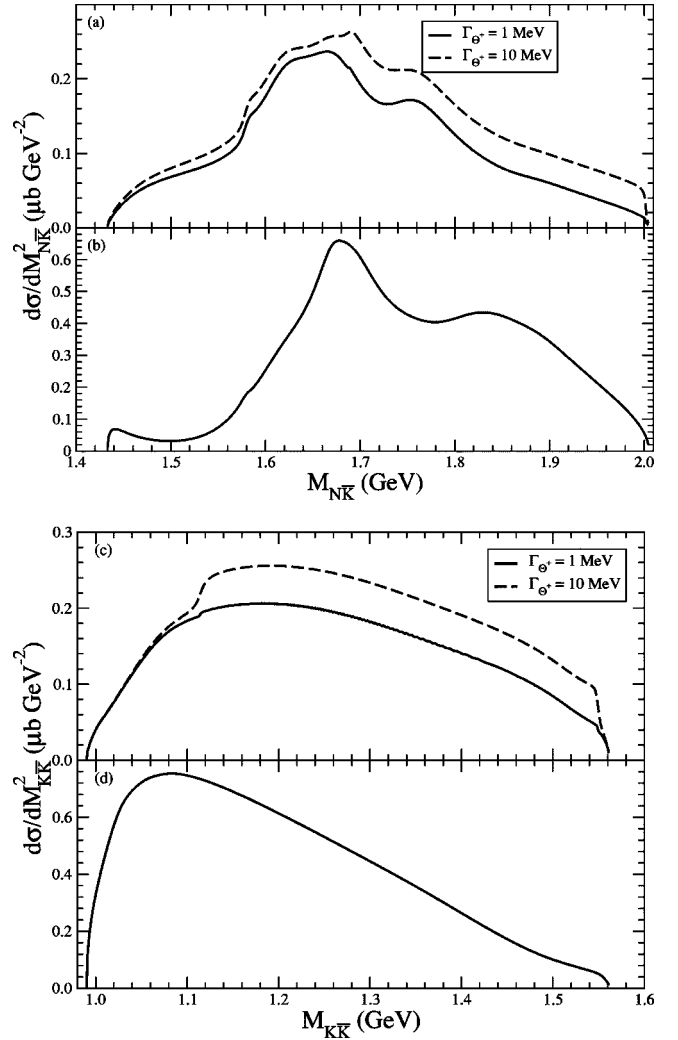


FIG. 12. The differential cross section $\partial\sigma/\partial M_{N\bar{K}}^2$ as a function of $M_{N\bar{K}}$ [(a) and (b)] and $\partial\sigma/\partial M_{K\bar{K}}^2$ as a function of $M_{K\bar{K}}$ [(c) and (d)]. The curves in (a) and (c) are for the process $\gamma n \to n K^+ K^-$, while those in (b) and (d) are for $\gamma p \to p K^+ K^-$.

up as large kinematic reflections. Figure 16 shows the cross sections for $p K^0 \bar{K}^0$ [(a) and (c)] and $n K^+ \bar{K}^0$ [(b) and (d)], both assuming a proton target. In all cases, both for positive [(a) and (b)] and negative [(c) and (d)] parity, the model indicates that clear, easy-to-isolate signals should be obtainable.

### 3. Integrated cross sections

In Ref. [3], in $\gamma d \to n p K^+ K^-$, 212 events are in the peak for the $\Lambda(1520)$, and there are 43 events in the peak of the $\Theta^+$. In addition, the Saphir Collaboration [4] report an estimated cross section of 200 nb for production of the $\Theta^+$ in the $\gamma p \to n K^+ \bar{K}^0$ channel. In this calculation, if we perform a numerical integration around the peak of the $\Lambda(1520)$, we find that the cross section in the peak in the channel $\gamma p \to p K^+ K^-$ is of the order of 300 nb, with some small fraction of this arising from nonresonant contributions. Table IV
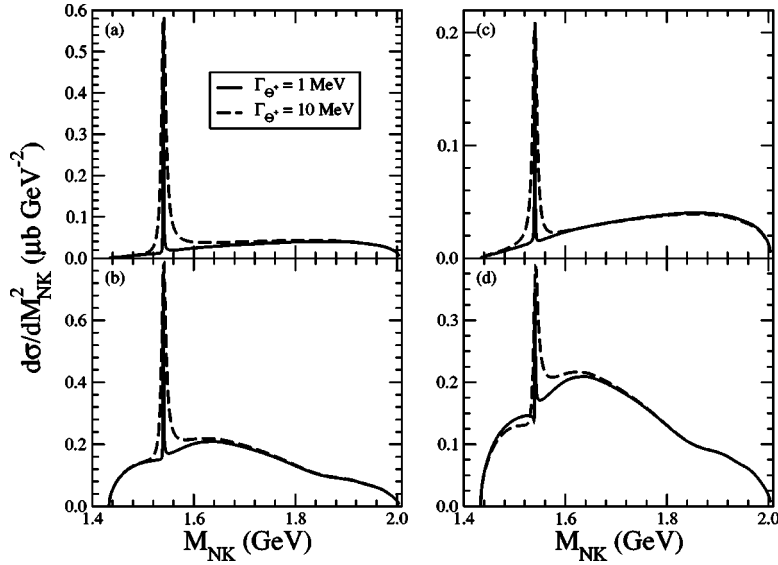
FIG. 13. The differential cross section $\partial\sigma/\partial M_{NK}^2$ as a function of $M_{NK}$. The curves in (a) and (c) are for the process $\gamma p \to pK^0\bar{K}^0$, while those in (b) and (d) are for $\gamma p \to nK^+\bar{K}^0$. (a) and (b) are for a positive parity $\Theta^+$ while (c) and (d) are for a $\Theta^+$ with negative parity.

shows the integrated cross section under the peak of the $\Theta^+$ for different channels in the different scenarios that we have explored. In each case, the integration is performed from $M-2\Gamma$ to $M+2\Gamma$, where $M$ is the mass of the $\Theta^+$ and $\Gamma$ is its width.

In each case, there is some contribution arising from "continuum" events that lie in the "right" kinematic regime. These continuum contributions represent a larger portion of the reported cross section for $1/2^-$ pentaquarks than for $1/2^+$ pentaquarks, for instance. For a $1/2^-$ pentaquark with a width of 10 MeV, approximately half of the reported 18 nb (in $\gamma n \to nK^+K^-$) arises from such continuum contributions. For a pentaquark with the same quantum numbers but a width of 1 MeV, approximately two-thirds of the reported 1.7 nb in the same channel are from the continuum.

Assuming that the number of events seen is directly proportional to the cross section, modulo questions of detector
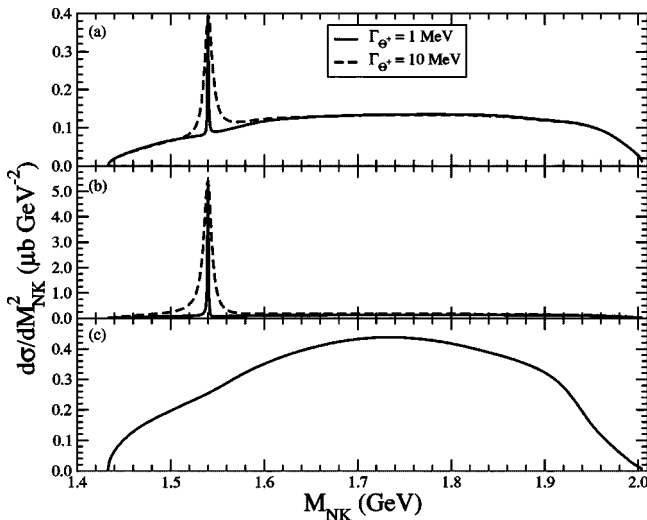




FIG. 14. The differential cross section $\partial\sigma/\partial M_{NK}^2$ as a function of $M_{NK}$, for a spin-3/2 $\Theta^+$. The curves in (a) and (b) are for the process $\gamma n \to nK^+K^-$, while (c) is for $\gamma p \to pK^+K^-$. In (a), the $\Theta^+$ has positive parity, while in (b), its parity is negative.
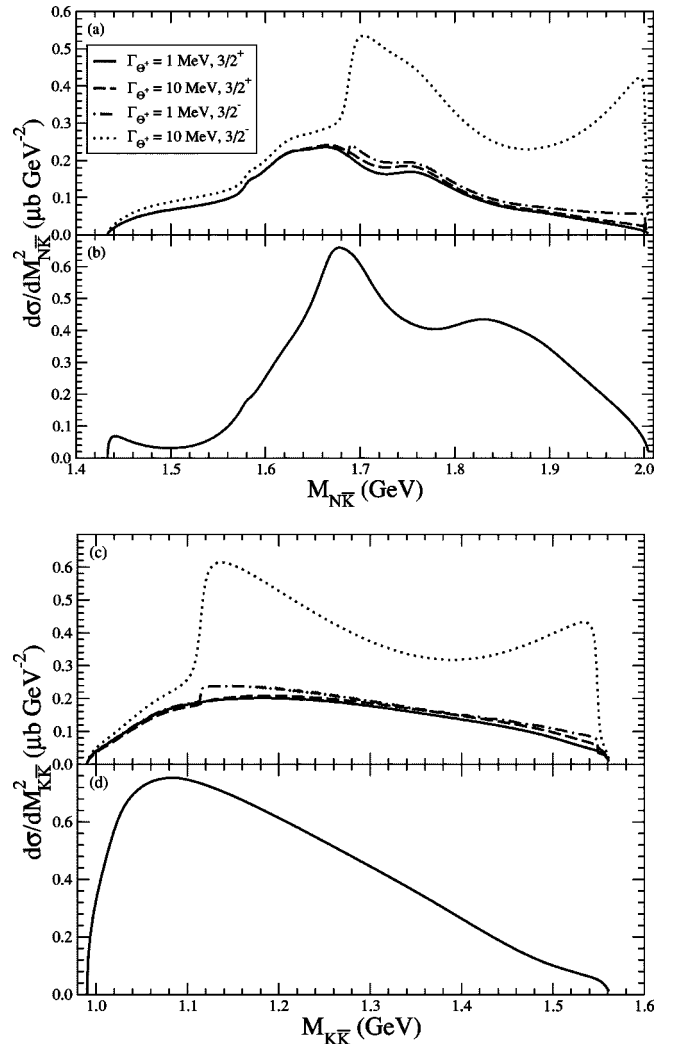
FIG. 15. The differential cross section as functions of $M_{N\bar{K}}$ [(a) and (b)] or $M_{K\bar{K}}$ [(c) and (d)]. The curves in (a) and (c) are for the process $\gamma n \to nK^+K^-$, while those in (b) and (d) are for $\gamma p \to pK^+K^-$.

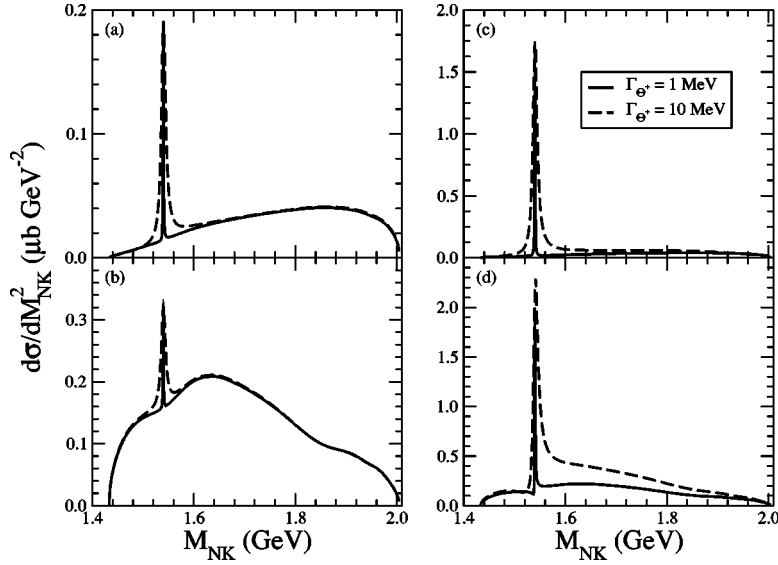FIG. 16. The differential cross section $\partial\sigma/\partial M_{NK}^2$ as a function of $M_{NK}$. The upper graphs are for the process $\gamma p \to pK^0\bar{K}^0$, while the lower ones are for $\gamma p \to nK^+\bar{K}^0$. Those on the left are for a $\Theta^+$ with positive parity, while those on the right assume negative parity for the pentaquark.

acceptances, resolution, and efficiencies, the JLab numbers suggest that the cross section for the $\Theta^+$ should be of the order of 60 nb around its peak in the channel $\gamma n \to nK^+K^-$.

The numbers in the table indicate that the versions of the model discussed so far are inconsistent with the $\Theta^+$ signal measured at Jefferson Lab, for instance. The estimated cross section inferred for production of the $\Theta^+$ in the process $\gamma n \to nK^+K^-$ is about 60 nb, and for a pentaquark with $J^P = 1/2^+$ and a width of 10 MeV, the cross section calculated in this model is 55 nb. However, such a large width for the state appears to be in contradiction to cross sections observed in other processes [18–23]: consistency with such observations would dictate that the preferred scenario is for a pentaquark with a width of 1 MeV. In this case, the scenario that most closely matches JLab observations is that with a $3/2^-$ pentaquark. However, the results of this calculation suggests that such a state should not need kinematic cuts for observation. None of the scenarios with the narrower $\Theta^+$ match the reported Saphir cross section of 200 nb.

We have examined cross sections for these processes at smaller values of $\sqrt{s}$. While the overall cross sections change, the relative strengths of various contributions remain similar to what they are at $\sqrt{s}=2.5$ GeV. In particular, the ratio of integrated cross section for the $\Theta^+$ and the $\Lambda(1520)$ remains similar to what it is at $\sqrt{s}=2.5$ GeV. Thus, the discrepancy between the results of our model and the signal seen at JLab would remain as difficult at lower energies.

### C. The role of the $K^*$

The preceding subsections suggest that, apart from the case of a $\Theta^+$ with $J^P=1/2^-$, a signal for this pentaquark should be readily observable, especially when the $\Lambda(1520)$ and $\phi$ are omitted from the calculation. However, there is still an inconsistency between what we have shown and what has been observed experimentally at JLab.

In the results presented, the contributions of the $K^*$ mesons have been limited to diagrams in which they couple only to ground-state hyperons and nucleons. At this point, there are no contributions in which the $K^*$ couple to excited hyperons, nor to the $\Theta^+$. It is relatively easy to include such contributions, and in so doing, we can increase the cross section for production of the $\Theta^+$.

The phenomenological Lagrangian for the coupling of the $\Theta^+$ to the $K^*$ may be written

$$\mathcal{L} = \bar{N}\left( G_v^{K^*N\Theta^+}\gamma^\mu K_\mu^* + \frac{G_t^{K^*N\Theta^+}}{M_N+M_{\Theta^+}}\gamma^\mu\gamma^\nu(\partial_\nu K_\mu^*)\right)\Theta + \text{H.c.,}$$

(26)

if the $\Theta^+$ is assumed to have $J^P=1/2^+$. This is the only scenario we discuss. The two coupling constants $G_v^{K^*N\Theta^+}$ and $G_t^{K^*N\Theta^+}$ are unknown. In Table V, we show results for different values of the vector coupling constant, with the tensor

TABLE IV. Total cross sections for production of the $\Theta^+$, in different scenarios, for the channels in which it can be produced. The numbers in the table are obtained from the versions of the model in which the $\phi$ and $\Lambda(1520)$ are omitted. The second to fifth columns in the table correspond to a $\Theta^+$ with a width of 1 MeV, while the sixth to ninth columns correspond to a width of 10 MeV.

| Process | $\sigma(\text{nb}), \Gamma_{\Theta^+}=1$ MeV | | | | $\sigma(\text{nb}), \Gamma_{\Theta^+}=10$ MeV | | | |
|---|---|---|---|---|---|---|---|---|
| | $1/2^+$ | $1/2^-$ | $3/2^+$ | $3/2^-$ | $1/2^+$ | $1/2^-$ | $3/2^+$ | $3/2^-$ |
| $\gamma p \to pK^0\bar{K}^0$ | 2.6 | 1.0 | 0.9 | 7.7 | 25.3 | 9.6 | 8.9 | 73.6 |
| $\gamma p \to nK^+\bar{K}^0$ | 4.3 | 2.4 | 2.3 | 10.0 | 44.8 | 27.9 | 26.0 | 110.5 |
| $\gamma n \to nK^+K^-$ | 5.6 | 1.7 | 2.2 | 24.0 | 54.5 | 18.0 | 22.8 | 229.9 |
| $\gamma n \to pK^0K^-$ | 5.9 | 1.8 | 2.0 | 24.0 | 56.1 | 19.0 | 21.2 | 225.1 |

TABLE V. Total cross sections for production of the $\Theta^+$, in different scenarios, for different processes. The numbers in the table are obtained from the versions of the model in which the $\phi$ and $\Lambda(1520)$ are omitted. All numbers assume that the $\Theta^+$ has $J^P=1/2^+$ and a width of 1 MeV. The tensor coupling is set to zero, and four different values of the vector coupling are used. All channels in which the $\Theta^+$ can be produced as a resonant state are shown.

| Process | $\sigma(\text{nb}), G_v^{K^*N\Theta^+}=2$ | $\sigma(\text{nb}), G_v^{K^*N\Theta^+}=4$ | $\sigma(\text{nb}), G_v^{K^*N\Theta^+}=6$ | $\sigma(\text{nb}), G_v^{K^*N\Theta^+}=8$ |
|---|---|---|---|---|
| $\gamma p \to pK^0\bar{K}^0$ | 32.7 | 125.9 | 282.2 | 502.8 |
| $\gamma p \to nK^+\bar{K}^0$ | 11.5 | 34.6 | 73.4 | 128.1 |
| $\gamma n \to nK^+K^-$ | 10.0 | 30.2 | 66.1 | 117.8 |
| $\gamma n \to pK^0K^-$ | 30.7 | 118.6 | 269.7 | 484.0 |

coupling set to zero. We see that relatively modest values of the vector coupling are sufficient to give a cross section of about 60 nb for production of the $\Theta^+$ in the $\gamma n \to nK^+K^-$ channel. However, even that modest value for the coupling constant (of about 6) is somewhat larger than values postulated by some authors. For instance, Close and Zhao [41] have suggested that $(G_v^{K^*N\Theta^+})^2 \approx 3$. In other models, similar values have been used. With $G_v^{K^*N\Theta^+}=6$, our model predicts a very large cross section of 280 nb for the production of the $\Theta^+$ in the $\gamma p \to pK^0\bar{K}^0$ channel, and a cross section of 73 nb in $\gamma p \to nK^+\bar{K}^0$. This means that, in this scenario, the contribution of the $K^*$ dominates the production of the $\Theta^+$. These numbers indicate that the reported JLab results are not consistent with the estimated Saphir cross section of 200 nb. In addition, in $pK^0\bar{N}^0$, the predicted cross section for production of the $\Theta^+$ is comparable to that for production of the $\Lambda(1520)$, implying that the signal should be easily observable.

## V. SUMMARY AND OUTLOOK

We have examined the process $\gamma N \to K\bar{K}N$ within the framework of a phenomenological Lagrangian. We have examined a number of scenarios for pentaquark production, and have found that the largest production cross section occurs for a $\Theta^+$ with $J^P=3/2^-$. However, in such a scenario, the cross section for its production is comparable to that for production of the $\Lambda(1520)$, and kinematic cuts should probably not be needed to enhance the signal.

If the $\Theta^+$ has $J^P=1/2^+$, the cross section for its production is significantly less than that for production of the $\Lambda(1520)$, by almost two orders of magnitude if its width is of the order of 1 MeV. This means that special mechanisms are required to account for the number of events seen in the JLab experiment, relative to the $\Lambda(1520)$. One possibility is that the coupling of the pentaquark to the $K^*$ is large, so that the dominant mechanism of production involves the $K^*$. However, this then leads to a signal for which kinematic cuts should not be necessary. One can also invoke the couplings

of a number of $N^*$ resonances, but the conclusion about the size of the signal would remain unchanged.

The only scenario (that we can think of) that would give the appropriate ratio between the cross section for production of the $\Lambda(1520)$ and the $\Theta^+$ is for the production of the $\Lambda(1520)$ to be suppressed even further than the suppression we have already obtained through the use of form factors. However, this seems unlikely, as the calculated cross section for producing this state is of the same order of magnitude as those published by Barber *et al.* [51].

## Outlook

This calculation is not without its shortcomings. The most important shortcoming is the fact that a very simple prescription has been employed to regulate the high-energy behavior of the model. A more realistic treatment, consistent with the requirements of gauge invariance, will have to be implemented before such a calculation is applied to other processes in the future.

There are prospects for measuring a number of final states with two pseudoscalar mesons at JLab and at other facilities. In particular, there are ongoing analyses of the processes $\gamma N \to \pi\pi N$, $\gamma N \to KK\Xi$, $\gamma N \to K\pi\Lambda$, and $\gamma N \to K\pi\Sigma$. The calculation we have presented has been set up in such a way that it may be applied to any of these (or other) processes in a relatively straightforward manner. The core of the code was originally generated for $\gamma N \to \pi\pi N$, and the modifications necessary for $\gamma N \to K\bar{K}N$ were not overly difficult. Thus, we may expect to apply the methods used herein to other processes in the not-too-distant future.

[1] LEPS Collaboration, T. Nakano *et al.*, Phys. Rev. Lett. **91**, 012002 (2003).

[2] DIANA Collaboration, V. Barmin *et al.*, Phys. At. Nucl. **66**, 1715 (2003) [Yad. Fiz. **66**, 1763 (2003)].

[3] CLAS Collaboration, S. Stepanyan *et al.*, Phys. Rev. Lett. **91**, 252001 (2003).

[4] SAPHIR Collaboration, J. Barth *et al.*, Phys. Lett. B **572**, 127 (2003).

[5] CLAS Collaboration, V. Kubarovsky *et al.*, Phys. Rev. Lett. **92**, 032001 (2004); **92**, 049902(E) (2004).

[6] A. E. Asratyan, A. G. Dolgolenko, and M. A. Kubantsev, Phys. At. Nucl. **67**, 682 (2004) [Yad. Fiz. **67**, 704 (2004)].

[7] HERMES Collaboration, A. Airapetian *et al.*, Phys. Lett. B **585**, 213 (2004).

[8] SVD Collaboration, A. Aleev *et al.*, hep-ex/0401024.

[9] COSY-TOF Collaboration, M. Abdel-Bary *et al.*, Phys. Lett. B **595**, 127 (2004).

[10] D. Diakonov, V. Petrov, and M. V. Polyakov, Z. Phys. A **359**, 305 (1997).

[11] NA49 Collaboration, C. Alt *et al.*, Phys. Rev. Lett. **92**, 042003 (2004).

[12] N. G. Kelkar, M. Nowakowski, and K. Khemchandani, nucl-th/0405008.

[13] H. G. Fischer and S. Wenig, hep-ex/0401014.

[14] HERA-B Collaboration, K. T. Knöpflet *et al.*, hep-ex/0403020.

[15] BES Collaboration, J. Z. Bai *et al.*, Phys. Rev. D **70**, 012004 (2004).

[16] S. Salur, nucl-ex/0403009.

[17] M. Karliner and H. J. Lipkin, Phys. Lett. B **597**, 309 (2004).

[18] S. Nussinov, hep-ph/0307357.

[19] R. A. Arndt, I. I. Strakovsky, and R. L. Workman, Phys. Rev. C **68**, 042201 (2003); **69**, 019901(E) (2004).

[20] J. Haidenbauer and G. Krein, Phys. Rev. C **68**, 052201 (2003).

[21] R. Cahn and G. Trilling, Phys. Rev. D **69**, 011501 (2004).

[22] W. R. Gibbs, nucl-th/0405024.

[23] A. Sibirtsev, J. Haidenbauer, S. Krewald, and Ulf-G. Meissner, Phys. Lett. B **599**, 230 (2004); nucl-th/0407011.

[24] A. R. Dzierba, D. Krop, M. Swat, S. Teige, and A. P. Szczepaniak, Phys. Rev. D **69**, 051901 (2004).

[25] R. Jaffe and F. Wilczek, Phys. Rev. Lett. **91**, 232003 (2003).

[26] S. Capstick, P. R. Page, and W. Roberts, Phys. Lett. B **570**, 185 (2003).

[27] B. K. Jennings and K. Maltman, Phys. Rev. D **69**, 094020 (2004).

[28] M. Karliner and H. J. Lipkin, Phys. Lett. B **575**, 249 (2003); **586**, 303 (2004).

[29] M. Karliner and H. J. Lipkin, hep-ph/0307343.

[30] Y. Kondo, O. Morimatsu, and T. Nishikawa, hep-ph/0404285; H. Kim, S. H. Lee, and Y. Oh, hep-ph/0404170; M. Eidemuller, hep-ph/0404126; S. L. Zhu, Phys. Rev. Lett. **91**, 232002 (2003); J. Sugiyama, T. Doi, and M. Oka, Phys. Lett. B **581**, 167 (2004).

[31] See, for example, Y. S. Oh and H. C. Kim, hep-ph/0405010; R. Bijker, M. M. Giannini, and E. Santopinto, hep-ph/0405195; hep-ph/0403029; H.-C. Kim and M. Praszalowicz, hep-ph/0405171; D. Melikhov, S. Simula, and B. Stech, hep-ph/0405037; N. I. Kochelev, H.-J. Lee, and V. Vento, hep-ph/0404065; J. J. Dudek, hep-ph/0403235; H.-Y. Cheng, C.-K. Chua, and C.-W. Hwang, Phys. Rev. D **70**, 034007 (2004); A. Zhang, Y.-R. Liu, P.-Z. Huang, W.-Z. Deng, X.-L. Chen, and S-L. Zhu, hep-ph/0403210; F. Stancu, hep-ph/0402044; F. Stancu and D. O. Riska, Phys. Lett. B **575**, 242 (2003); C. Carlson *et al.*, *ibid.* **579**, 52 (2004).

[32] M. Bando, T. Kugo, A. Sugamoto, and S. Terunuma, hep-ph/0405259; A. Sugamoto, hep-ph/0404019.

[33] D. Akers, hep-ph/0403142; X.-C. Song and S.-L. Zhu, hep-ph/0403093.

[34] P. Bicudo, hep-ph/0405254; P. Bicudo, hep-ph/0405086; P. Bicudo and G. M. Marques, hep-ph/0312391; M. Nunez, S. Lerma, P. O. Hess, S. Jesgarz, O. Civitarese, and M. Reboiro, Phys. Rev. C **70**, 025201 (2004).

[35] F. J. Llanes-Estrada, E. Oset, and V. Mateu, Phys. Rev. C **69**, 055203 (2004).

[36] F. Csikor, Z. Fodor, S. D. Katz, and T. G. Kovacs, J. High Energy Phys. **11**, 070 (2003).

[37] S. Sasaki, hep-lat/0310014.

[38] T. W. Chiu and T. H. Hsieh, hep-ph/0403020.

[39] N. Mathur *et al.*, hep-ph/0406196.

[40] M. V. Polyakov and A. Rathke, Eur. Phys. J. A **18**, 691 (2003).

[41] F. E. Close and Q. Zhao, Phys. Lett. B **590**, 176 (2004).

[42] T. Hyodo, A. Hosaka, and E. Oset, Phys. Lett. B **579**, 290 (2004).

[43] S. I. Nam, A. Hosaka, and H.-Ch. Kim, Phys. Lett. B **579**, 43 (2004); hep-ph/0403009.

[44] W. Liu and C. M. Ko, Phys. Rev. C **68**, 045203 (2003); nucl-th/0309023.

[45] Y. Oh, H. Kim, and S. H. Lee, Phys. Rev. D **69**, 074016 (2004); **69**, 014009 (2004); hep-ph/0312229.

[46] Q. Zhao, Phys. Rev. D **69**, 053009 (2004).

[47] Q. Zhao and J. S. Al-Khalili, Phys. Lett. B **585**, 91 (2004).

[48] B.-G. Yu, T.-K. Choi, and C.-R. Ji, Phys. Rev. C **70**, 045205 (2004).

[49] K. Nakayama and K. Tsushima, Phys. Lett. B **583**, 269 (2004).

[50] S. Eidelman *et al.*, Phys. Lett. B **592**, 1 (2004).

[51] D. P. Barber *et al.*, Z. Phys. C **7**, 17 (1980).